HHS Public Access

Author manuscript

Phys Med Biol. Author manuscript; available in PMC 2018 November 29.

Published in final edited form as:

Phys Med Biol. ; 62(24): 9341–9356. doi:10.1088/1361-6560/aa96d0.

Electromechanical wave imaging and electromechanical wave velocity estimation in a large animal model of myocardial infarction

Alexandre Costet, MSc[1], **Lea Melki, MS**[1], **Vincent Sayseng, MS**[1], **Nadira Hamid, MD**[2], **Koki Nakanishi, MD**[2], **Elaine Wan, MD**[2], **Rebecca Hahn, MD**[2], **Shunichi Homma, MD**[2], and **Elisa Konofagou, PhD**[1,3]

[1]Department of Biomedical Engineering, Columbia University, New York, NY, USA

[2]Department of Medicine - Division of Cardiology; College of Physicians and Surgeons, Columbia University, New York, NY. USA

[3]Department of Radiology, Columbia University, New York, NY, USA

Abstract

Background—Echocardiography is often used in the clinic for detection and characterization of myocardial infarction. Electromechanical wave imaging (EWI) is a non-invasive ultrasound-based imaging technique based on time-domain incremental motion and strain estimation that can evaluate changes in contractility in the heart. In this study, electromechanical activation is assessed in infarcted heart to determine whether EWI is capable of detecting and monitoring infarct formation. Additionally, methods for estimating electromechanical wave (EW) velocity are presented, and changes in the EW propagation velocity after infarct formation are studied.

Methods and Results—Five (n=5) adult mongrels were used in this study. Successful infarct formation was achieved in three animals by ligation of the left anterior descending (LAD) coronary artery. Dogs were survived for a few days after LAD ligation and monitored daily with EWI. At the end of the survival period, dogs were sacrificed and TTC (Tetrazolium chloride) staining confirmed the formation and location of the infarct. In all three dogs, as soon as day 1 EWI was capable of detecting late-activated and non-activated regions, which grew over the next few days. On final day images, the extent of these regions corresponded to the location of infarct as confirmed by staining. EW velocities in border zones of infarct were significantly lower post-infarct formation when compared to baseline, whereas velocities in healthy tissues were not.

Conclusions—These results indicate that EWI and EW velocity might help with the detection of infarcts and their border zones, which may be useful for characterizing arrhythmogenic substrate.

Introduction

Coronary heart disease and myocardial infarction (MI) were responsible for 1 out of every 7 deaths in the US in 2011, and it is estimated that, each year, approximately 635,000

Correspondence to: Dr. Elisa Konofagou, 1210 Amsterdam Ave., ET 351, MC 8904, New York, NY, 10027, ek2191@columbia.edu | Phone: 212-342-0863 | Fax: 212-342-1648.

Americans are hospitalized due to MI [1]. In the clinic, MI diagnosis is based on elevated cardiac enzyme levels such as Creatine Phosphokinase and Troponin [2,3] and abnormal electrocardiogram (ECG) features such as ST segment elevation or depression and pathological Q waves [4]. Assessment of MI is commonly performed by single-photon emission computerized tomography, ultrasound imaging, nuclear imaging (radionuclide angiography, perfusion imaging, positron emission tomography), magnetic resonance imaging (MRI), or a combination thereof [5–8]. Most of the aforementioned techniques, however, either involve ionizing radiation or are contraindicated for patients with pacemakers or stents. Echocardiography is currently the preferred method for the assessment of patients with MI, mainly due to its portability and ubiquity in the clinic. Echocardiography is used for wall motion scoring, to detect leaks or septal defects, as well as during stress tests. Over the past two decades, several new ultrasound-based methods have been developed to estimate displacement and deformation. In particular, speckle-tracking motion and strain estimation based on Bmode [9] or radio-frequency (RF) ultrasound signals [10–13] have been developed and are in use on clinical scanners. Such techniques are used for detection of contractility changes in the myocardium aimed at ischemia and infarct detection.

Electromechanical Wave Imaging (EWI) is one of such techniques. EWI is a non-invasive, non-ionizing, ultrasound-based imaging modality that can map the electromechanical activity of the heart in all four chambers at a high spatial and temporal resolution, with real-time feedback capabilities [13–18]. EWI relies on high framerate, time-domain, RF signal speckle-tracking techniques to estimate minute displacements and incremental (or inter-frame) axial strains in the myocardium during systole. At the tissue level, the electrical activation of the heart consists of the depolarization of cardiac cells via propagation of action potentials. Following a delay of a few tens of milliseconds [19,20], this depolarization triggers the electromechanical activation, i.e., the first time-point at which the muscle transitions from a relaxation to a contraction state. Using incremental strain estimation in the axial direction, EWI tracks the electromechanical wave (EW) which refers to the spatial propagation of the electromechanical activation through the heart. Previous studies have shown that the EW propagation is highly correlated with the underlying electrical activation sequence in all four chambers of the heart in normal canine hearts during sinus rhythm and various pacing protocols *in silico* and *in vivo* [15,21–23]. EWI has also been shown capable of localizing regions of ischemia in a large animal model during intermediate levels of occlusion of the left anterior descending artery (LAD) [13], but not yet for detection and monitoring of MI.

In this study, we propose to use EWI to assess the electromechanical activation, or lack thereof, in infarcted hearts. The goal is to determine whether EWI is capable of detecting infarction in the heart and of monitoring MI formation. Additionally, for the first time, we introduce and implement new processing methods to estimate 2D EW velocity field in order to assess the changes in propagation velocity of the electromechanical activation after infarct formation. In order to reach this goal, a large animal model of MI was used. MI was achieved by ligating the LAD of adult mongrel dogs and surviving the animals for up to 5 days to allow for MI formation. During this process, daily EWI acquisitions were performed and pseudo 3D maps of the electromechanical activation times, or isochrones, were

generated. EW velocity was estimated and compared in both healthy myocardial regions and border zones of infarct pre- and post-infarct formation. On the last day, the animals were sacrificed and the heart excised and stained in order to determine the location of the infarct and compare it to the location detected on the pseudo 3D EWI isochrones.

Methods

Experimental protocol

This study complied with the Public Health Service Policy on Humane Care and Use of Laboratory Animals and was approved by the Institutional Animal Care and Use Committee of Columbia University. In order to determine reproducibility of results, we needed to create a region of infarct in at least two dogs. Because dogs are well known for developing collateral coronary circulation in the event of coronary obstruction [24] which can prevent the formation of an infarct, and based on insights from the veterinarians at Columbia University's Institute of Comparative Medicine, for this study we chose to use five adult male mongrel dogs (n=5) weighting 22.6 ± 0.6 kg in order to guarantee the formation of an infarct in at least two animals. No randomization was used in this study as we aimed for the creation of an infarct in all animals and, as a result, there was no blinding of investigators involved. Following transthoracic baseline EWI acquisitions performed prior to surgery, anesthesia was induced and the left side of the chest of the dogs was clipped and surgically prepped. Then, lateral thoracotomy was performed to expose the heart, the pericardium was incised and the proximal LAD artery was dissected free. The dissection was followed by a 2-stage ligation on the LAD with a 2.0 silk suture in order to create an anteroseptal MI [25]. The thoracotomy incision was then repaired in layers with 2.0 Vicryl absorbable sutures and the skin closed with surgical staples. A chest tube was placed to achieve negative intrathoracic pressure and removed immediately after evacuating the chest. After surgery, dogs were recovered from anesthesia and returned to the animal facilities for postoperative care which included antiarrhythmic drugs, antibiotics and pain management. Dogs were checked and assessed for pain hourly after surgery through the night, until the next morning. Daily EWI acquisitions were performed during the monitoring period. After survival of the animals for 4 to 5 days, anesthesia was induced and one last EWI acquisition was performed, transthoracically, before euthanasia. The heart was then removed in order to assess the extent of the infarct via Tetrazolium Chloride (TTC) staining. For staining, the excised heart was sectioned in short-axis slices approximately 5 mm thick which were covered in 1% TTC solution and kept at 37°C for 15 to 20 minutes. The slices were then submerged in 10% Formalin solution for 5 minutes. If no infarct is confirmed with staining, the results from the animal will be excluded.

Electromechanical Wave Imaging

EWI was acquired prior to surgery, each day during monitoring, and on the last day prior to sacrifice. All acquisitions were performed transthoracically on closed-chest dogs in four apical views: 3 standard apical echocardiographic views (4-chamber, 2-chamber, and 3-chamber), and an additional view, the "3.5-chamber" view, acquired in between the 2- and 4-chamber views. Previous study by our group based on the theoretical framework of the Strain Filter [26] found that the optimal motion-estimation rate for EWI is between 500 and

2000 Hz [16]. As a result, an unfocused transmit sequence was used on a Verasonics system (Verasonics, Redmond, WA) in order to acquire ultrasound RF frames at 2000 fps using a 2.5-MHz ATL P4-2 phased array. Such a high frame rate can be achieved by emitting unfocused circular ultrasound waves using a virtual focus located 10.2 mm behind the array (Figure 1-1) [15]. This allowed us to reach a high framerate while being able to get a full view of the heart for each transmit for the purpose of EWI. Owing to the fact that the B-mode images reconstructed from these unfocused transmit sequences have lower resolution and signal-to-noise ratio than the images obtained from traditional focused beam sequences, which results in a challenging segmentation process, a standard 64-line B-mode acquisition was performed following the initial high frame rate acquisition. The complete acquisition sequence consisted of 2 s of high frame rate acquisition at 2000 fps (4000 frames acquired), followed by an anatomical imaging sequence consisting of 1.5 s of a standard 64-line B-mode acquisition at 30 fps. An ECG was acquired simultaneously during all ultrasound acquisition and the ECG acquisition was triggered by the first ultrasound wave emission. Retrospective ECG-gating was used in order to temporally align the high frame rate acquisition used in EWI with the anatomical B-mode acquisition. Briefly, EWI sequence and B-mode acquisition were temporally aligned by using periodic ECG features such as the QRS complex and up-sampling the B-mode framerate to 2000 fps (Figure 1-1).

Beamforming on the element data obtained from each of the probe's elements was performed during post-processing using a sum-and-delay algorithm, resulting in the reconstruction of one RF (radio-frequency) frame per transmit. RF frames denote the beamformed, unprocessed and unfiltered ultrasound images that contain the phase information that is lost when generating B-mode images. RF frames were used for motion and strain estimation as RF-based speckle tracking techniques have be shown to offer far greater accuracy than B-mode speckle tracking techniques [27]. The reconstructed RF images had an angular sampling of 0.7° or 0.025 rad (128 lines spanning 90°) and an axial sampling frequency of 20 MHz (axial sampling of 0.0385 mm) (Figure 1-2). The axial direction here is defined with respect to standard apical echocardiography views, i.e., the lines that spread out from the probe at the apex of the heart (top of the image) to the base of the heart (bottom of the image). Segmentation of the myocardium was manually performed on the first frame of the anatomical B-mode sequence and the endocardial contour was subsequently automatically tracked through the cardiac cycle using the estimated displacements [28]. Displacement estimation was performed using a fast, 1D RF-based cross-correlation algorithm with overlapping 6.2 mm axial windows (10 wavelengths) and a 0.62 mm window shift (90% overlap) [29] (Figure 1-3). Axial incremental strains (i.e. the change in cumulative strain in the axial direction) were estimated using a least-squares estimator with a 5-mm, 1D-kernel [30] (Figure 1-4). Strain estimates were then filtered using a 12 mm by 10 beams, moving-average spatial filter and a temporal low-pass filter with a 125-Hz cut-off frequency. The displacement and strain estimations were both performed in polar coordinates and the results were subsequently converted to Cartesian coordinates.

Remembering that the incremental strain corresponds to the change in cumulative strain between two consecutive frames, electromechanical activation was defined as the time at which the incremental strain value changes from positive (increase in cumulative strain, i.e.,

lengthening in the axial direction) to negative (decrease in cumulative strain, i.e., shortening or contraction in the axial direction), that is, crosses zero (Figure 1-4). Based on this definition of the electromechanical activation, we subsequently generated isochrones by mapping the first occurrence of the incremental strain crossing zero in the ventricles after the onset of the QRS (positive to negative values, i.e., onset of contraction). The zero-crossing timings were semi-manually obtained in 60 to 100 randomly selected regions. Regions for which the incremental strain curve did not show any zero-crossings during the selected cardiac cycle were marked as "non-activating" and denoted by the color black on activation maps. A sub-sample resolution was obtained through cubic spline interpolation, and smooth continuous isochronal maps were then generated through a Delaunay triangulation-based cubic interpolation. Finally, all views were co-registered in Amira 5.3.3 (Visage Imaging, Chelmsford, MA, USA), both temporally (using ECG) and spatially (using B-mode anatomical landmarks such as the position of the valves and apex), to generate pseudo 3D isochrones (Figure 1-5).

EW velocity estimation

Previous work by our group estimated the propagation velocity of the electromechanical wave in mice in one dimension along the longitudinal wall by tracking the wavefront of propagation, estimating the distance traveled, and dividing it by the time elapsed [14]. The wavefront propagation, however, occurs in two dimensions on the 2D slices we obtain with EWI, and as a result we need a method to estimate the velocity vector field. The method we chose is adapted from previous work from Bayly et al. [31] and relies on fitting a polynomial surface to 2D activation data. This method was chosen due to its robustness to noise and missing points, and because it is well-adapted to any arrangement of points [32]. A block diagram of the methodology is presented in Figure 2. First, EWI isochrones were generated and each point on the isochrones is labeled by its coordinates in space and time: $z_i = (x_i, y_i, t_i)$. Second, the EW velocity vector field was estimated at every point z_i within the region of interest by fitting a smooth polynomial surface to a region on the activation wavefront within a specified neighborhood of points centered in space and time on z_i, and characterized by the parameters Δx, Δy, and Δt. The smooth polynomial surface was fitted using a least-square algorithm implemented in the Matlab function "fit'. The fitted surface describes activation times as a function of the position. In this study, the neighborhood of points was defined by the value of the parameters: $\Delta x = \Delta y = 10$ pixels and $\Delta t = 5$ms. These values were chosen so that the window size for the fit was at least four to five times the sampling interval in each dimension in order to guarantee that the variance in x, y and t due to propagation is much larger than the variance due to noise and measurement imprecision [31]. We also required a minimum of 20 points in the window for the fit, and a "good fit" criteria was defined which required $R^2 \geq 0.8$ and RMSE ≤ 5. If the neighborhood of points for the fit did not include at least 20 points or if the fit did not meet the "good fit" criteria, the current considered point was discarded (Figure 2-2). The velocity vector field was then estimated by solving the equation presented on Figure 2-3 for each point within the region of interest. Videos depicting the progression of the EW and its velocity vectors may also be generated from the velocity vector field by overlaying the vectors on the activation wavefront with the length of the vectors being proportional to the velocity (Figure 2-3).

In this study, since the regions of infarct were anteroseptal we estimated EW velocities on 2-chamber views prior to and after MI formation. Pre- and post-MI formation EW velocities were compared in both a healthy region and a border zone of infarct. The healthy region was chosen as a posterior region in which the activation pattern did not change after infarct formation while the border zone was defined as an anterior late-activated region located right next to a non-activated region (Figure 7).

Statistical analysis

EW velocity values are presented as mean ± standard deviation. A two-tailed Student's t-test was used to determine significant difference ($p < 0.05$) between velocities before and after MI formation.

Results

Electromechanical wave imaging

The success rate of MI formation was 60%. Two (n=2) of the five animals did not develop a MI after LAD ligation (Figure 3, Dogs #2 and #3). Figures 4, 5 & 6 depict EWI results for each of the dogs for which a MI formed as confirmed by histology (which corresponds to dogs #1, #4, and #5). Figure 7 shows EW velocity results.

Figure 4 depicts the EWI maps for dog #1. Pseudo 3D EWI isochrones of the electromechanical activation are presented on the left while staining results are presented on the right. Prior to surgery (day 0), electromechanical activation was uniform across the ventricles. Late-activated regions could be seen as soon as day 1, mostly located in the apical region. On day 2, late-activated regions (in blue) and non-activated regions (in black) were depicted anteriorly. On day 3, these regions had grown in size and non-activated regions could clearly be seen on the anterior and anteroseptal walls near the apex and from mid-level to apex, respectively. On the last day before sacrifice, a region located anteriorly and extending from the septum to the lateral wall and from the mid-level to the apex was activated after the remainder of the ventricle. There were also a few regions that did not activate: on the anterior wall from mid-level to apex and anteroseptal just below the mid-level and near the apex. Staining confirmed the location of the MI as being mostly anterior/anteroseptal near the apex, spreading to the lateral side near the mid-level.

Figure 5 depicts EWI maps in dog #4. Pseudo 3D EWI isochrones of the electromechanical activation are presented on the left while staining results are presented on the right. EWI isochrones before ligation showed the ventricles activating uniformly. For this animal, LAD ligation leads to temporary cardiac arrest during surgery. The animal was successfully revived and monitored closely for 4 days following the surgery. As soon as day 1, the heart exhibited extensive non-activated regions: on the anterior, anterior-lateral, and lateral wall. The anteroseptal wall show late activation compared to the rest of the ventricles. Day 2 isochrones showed a very similar pattern of activation with late-activated and non-activated regions depicted anteriorly and laterally. On day 3, the lateral wall appeared to recover from basal to mid-level while the anterior, anteroseptal and anterior-lateral wall as well as the apex showed late activation and non-activated regions. On the last day, the late-activated and

non-activated regions were located anteriorly from septum to lateral side. Histology results showed location of the MI anteriorly from apex to just below the ligation, and on the septum and lateral side from the mid-level to the apex.

Figure 6 depicts EWI maps for dog #5. Pseudo 3D EWI isochrones of the electromechanical activation are presented on the left while staining results are presented on the right. Similar to results in the other dogs, pre-surgery EWI isochrones showed most of the ventricles activating uniformly. By day 1, the apex activated late and the lateral wall near the apex showed non-activated regions. On day 2, the lateral wall mostly recovered while the apex and anterior side of the heart, mostly from mid-level to apex, depicted late-activated regions as well as a few non-activated regions. On the final day before sacrifice, late and non-activated regions were depicted apically and anteriorly from the septum to the lateral side of the heart. These results were corroborated by the staining which showed MI being located at the apex and anteriorly from septum to lateral side and from apex to mid-level.

EW velocity

Figure 7 depicts results of the EW velocity estimation. For each of the dogs considered, the red and green circles indicate the regions in which the EW velocities were extracted for comparison. In the healthy regions, we did not find a statistical significant difference in the EW velocity values before and after infarct formation. In the border zone of the infarct, we found a statistically significant difference in EW velocity values before and after infarct formation.

Discussion

In this study, we investigated using EWI to assess and monitor MI formation in a large animal model. EWI relies on detecting minute displacements and strains in order to map the onset of the deformation that follows the electrical activation. The electromechanical activation has been previously shown to follow the same pattern of activation as the electrical activation [15,21,22]. However, during ischemia and infarct the electromechanical coupling unravels. Indeed, the LAD coronary artery supplies the anterior side of the heart from the anteroseptal side to the anterior-lateral side as well as the apex [33]. Ligation of the LAD effectively creates ischemia in such regions. Changes in the myocardium are almost immediate as biochemical and functional abnormalities occur almost 60 seconds after the onset of ischemia. Furthermore, irreversible injury can occur within 20 to 40 minutes in the case of total blood flow occlusion [33]. Prolonged ischemia leads to cardiac cell death and the formation of an infarct. This results in a reduced contractility and, as a result, a decoupling of the electrical activation and its induced mechanical response.

The electromechanical uncoupling that takes place during ischemia and infarct may be perceived as a formidable challenge for EWI to image MI. However, this study shows that this was not the case. Indeed, the reduced movement or deformation may also yield insight into the electromechanical activation. This study showed that EWI was capable of accurately imaging akinesis and hypokinesis, i.e, regions that do not contract or contract later than the rest of the heart. Furthermore, we showed that these regions corresponded to regions of infarct as confirmed by TTC staining. EWI results presented here also showed a progression

in the formation of MI. For example, in dog #1 (Figure 4), the first isochrone after ligation showed an activation pattern through the ventricles that was less uniform than the one prior to ligation. Over the next two days, the late- and non-activated regions grew in size and the final map taken before sacrifice showed late- and non-activated regions where staining confirmed MI. These results indicate that EWI is capable of not only detecting MI and ischemia, but also to monitor the expansion of such regions. This suggests that EWI may be helpful as a diagnostic and monitoring tool to non-invasively assess the extent of ischemia and infarct in the clinic.

Border zones of infarct are characterized by slower conduction speeds and abnormal mechanics. Indeed, previous studies of the electromechanical coupling in infarcted hearts using MRI and an electrode sock around the heart found that there was a significant delayed activation within the infarct zone, and that regions of infarct had abnormal mechanics: notably a loss of the transmural gradient of the radial, circumferential and longitudinal strains which extended far beyond the infarct zone into what is called the border zone of infarct [34]. These changes stem from structural and electrophysiological changes in tissue near the infarct. Indeed, the directional differences in electrical activation propagation, which exists in healthy tissue, disappear after two weeks post-MI formation, and fibrosis leads to separation and distortion of the muscle fibers which impact the mechanical properties of the myocardium [36,37]. Furthermore, the slow conduction speed in border zones of infarct is due to the combination of fewer gap junctions impeding the propagation of the depolarization, and diminished connections between the cells due to fibrosis [36,37].

In this study, we found late-activated regions near the regions of infarct that also showed significantly lower EW velocities. These regions may correspond to the border zone of infarct as late activation and slow velocities might be the direct results of slower conduction speed and electromechanical decoupling. Thus, EWI may be capable of identifying these border zones by using a combination of EWI isochrones (for abnormal mechanics) and EW velocity estimation (to detect regions of slow conduction). This is of particular interest clinically since infarct border zones are believed to be a substrate for arrhythmogenesis due to the persistence of slow conduction, altered gap junctions, and anisotropy in tissue structure which may give rise to reentrant circuits and ventricular tachycardia [36,38–40]. Furthermore, the extent of the border zone has been found to be a strong predictor of post-MI ventricular arrhythmia and mortality [41,42]. Higher standard deviations of the velocity values were found in healthy tissue regions when compared to velocities in the border zone of infarct. This high standard deviation value may be due to the fact that healthy tissue is typically more mobile and as such may undergo more deformation than tissue in the border zone of infarct. Because healthy tissue is typically surrounded by healthy tissue, tethering due to neighboring tissue contracting may result in local regions of healthy tissue appearing to be deforming and moving more slowly by virtue of having to “fight” against already contracting tissue. As a result, there may be a bigger spread of velocities in healthy tissue regions, thus contributing to a higher standard deviation value.

To our knowledge, this is the first time that EWI has been used to detect regions of infarct. Previous work by our group used myocardial elastography to detect and assess infarction in mice [43] and showed that cumulative strain was capable of differentiating between normal

and infarct myocardium. Myocardial elastography is capable of assessing the mechanical function (and dysfunction) of the cardiac tissue but, owing to the fact that it relies on end-systolic values of the cumulative strain, does not provide information on the timeline of the mechanical activation following the electrical activation. On the other hand, EWI is capable of providing insights into the delay between the electrical and mechanical activation of the tissue which may help localize border zones of infarct and arrhythmogenic regions.

Limitations of this study include the fact that EWI is a 2D modality that relies on 1D motion and strain estimation, and that is used to map 3D propagation. One solution to this problem is to acquire multiple 2D views in order to capture the 3D propagation pattern. These slices can then be used to generate pseudo 3D isochrones which may provide a sufficient sampling of the 3D propagation pattern. EW velocity estimation is particularly impacted by this limitation which results in large standard deviations. Indeed, when the propagation wavefront come into the field of view of the 2D slice, the initial velocities at these points tend to be very large due to the fact that EW velocity estimation relies on a gradient operator. The criteria for a good fit and the number of points in the neighborhood of the fit mitigate this problem but further study of the influence of the parameters need to be conducted. Additionally, 3D EWI may also help with this issue and is currently being investigated by our group. Another limitation of this study could arise from the fact that the pseudo 3D electromechanical activation isochrones are generated from four different acquisitions. This was not deemed as a concern in this study because we were performing EWI in the case of a stable rhythm (here, sinus rhythm) and because we have previously shown EWI to be reproducible and repeatable between heart cycles both within the same acquisition and between separate acquisitions [17,18]. This is, however, an issue that should be considered when using EWI for imaging arrhythmias. Additionally, EWI isochrones only provide contraction information over one heartbeat which limits long-term change analysis referenced to a common time point. One possible solution would be to average isochrones over multiple heart beats at different time point during the experiment (eg: pre-ligation, post-ligation, 1-day after ligation, etc) and compare resulting averaged isochrones to be able to detect long-term changes trend.

Conclusion

In this study, we investigated using EWI to diagnose and assess infarction in a large animal model. We showed that EWI was capable of detecting infarcted regions in the heart, and that EWI could also monitor the formation of a MI over several days. The location of the MI as determined with EWI was confirmed by TTC staining. Additionally, for the first time, we introduced and implemented a new processing method for EW velocity estimation. We found that EW velocities in the border zone of infarct were significantly lower when compared to pre-MI values. These results suggest that using a combination of EWI and EW velocity maps may help with the detection of MI and of the border zones of infarct, which may be useful for the prediction of arrhythmia in the clinic.

Acknowledgments

This work was supported in part by the National Institutes of Health (R01EB006042, R01HL114358). Dr. Elaine Wan is supported by the Gerstner Scholars Program and is an endowed Esther Aboodi Assistant Professor at Columbia University.

References

1. Benjamin, EJ., Blaha, MJ., Chiuve, SE., Cushman, M., Das, SR., Deo, R., et al. Heart Disease and Stroke Statistics—2017 Update: A Report From the American Heart Association. Circulation [Internet]. 2017. Jan 1. [cited 2017 Apr 19]; Available from: http://circ.ahajournals.org/content/early/2017/01/25/CIR.0000000000000485
2. Ishihara M, Nakao K, Ozaki Y, Kimura K, Ako J, Noguchi T, et al. Long-Term Outcomes of Non-ST-Elevation Myocardial Infarction Without Creatine Kinase Elevation - The J-MINUET Study. Circ J Off J Jpn Circ Soc. 2017 Mar 17.
3. Sharma D, Gupta P, Srivastava S, Jain H. Sensitivity and specificity of cardiac troponin-T in diagnosis of acute myocardial infarction. Int J Adv Med. 2017 Jan 23; 4(1):244–6.
4. Thygesen K, Alpert JS, White HD. Universal Definition of Myocardial Infarction. J Am Coll Cardiol. 2007 Nov 27; 50(22):2173–95. [PubMed: 18036459]
5. Cavender MA, Bhatt DL, Stone GW, White HD, Steg PG, Gibson CM, et al. Consistent Reduction in Peri-Procedural Myocardial Infarction with Cangrelor as Assessed by Multiple Definitions: Findings from CHAMPION PHOENIX. Circulation. 2016 Aug 1. CIRCULATIONAHA. 115.020829.
6. Hillenbrand HB, Kim RJ, Parker MA, Fieno DS, Judd RM. Early assessment of myocardial salvage by contrast-enhanced magnetic resonance imaging. Circulation. 2000 Oct 3; 102(14):1678–83. [PubMed: 11015347]
7. Layland J, Oldroyd KG, Curzen N, Sood A, Balachandran K, Das R, et al. Fractional flow reserve vs. angiography in guiding management to optimize outcomes in non-ST-segment elevation myocardial infarction: the British Heart Foundation FAMOUS–NSTEMI randomized trial. Eur Heart J. 2015 Jan 7; 36(2):100–11. [PubMed: 25179764]
8. Abbott BG, Abdel-Aziz I, Nagula S, Monico EP, Schriver JA, Wackers FJ. Selective use of single-photon emission computed tomography myocardial perfusion imaging in a chest pain center. Am J Cardiol. 2001 Jun 15; 87(12):1351–5. [PubMed: 11397352]
9. Li Y, Garson CD, Xu Y, Beyers RJ, Epstein FH, French BA, et al. Quantification and MRI Validation of Regional Contractile Dysfunction in Mice Post Myocardial Infarction Using High Resolution Ultrasound. Ultrasound Med Biol. 2007 Jun; 33(6):894–904. [PubMed: 17434660]
10. D'hooge J, Konofagou E, Jamal F, Heimdal A, Barrios L, Bijnens B, et al. Two-dimensional ultrasonic strain rate measurement of the human heart in vivo. Ultrason Ferroelectr Freq Control IEEE Trans On. 2002; 49(2):281–286.
11. Sutherland GR, Di Salvo G, Claus P, D'hooge J, Bijnens B. Strain and strain rate imaging: a new clinical approach to quantifying regional myocardial function. J Am Soc Echocardiogr. 2004 Jul; 17(7):788–802. [PubMed: 15220909]
12. Lee WN, Provost J, Fujikura K, Wang J, Konofagou EE. In vivo study of myocardial elastography under graded ischemia conditions. Phys Med Biol. 2011; 56:1155. [PubMed: 21285479]
13. Provost J, Lee W-N, Fujikura K, Konofagou EE. Electromechanical Wave Imaging of Normal and Ischemic Hearts In Vivo. IEEE Trans Med Imaging. 2010 Mar; 29(3):625–35. [PubMed: 19709966]
14. Konofagou EE, Luo J, Saluja D, Cervantes DO, Coromilas J, Fujikura K. Noninvasive electromechanical wave imaging and conduction-relevant velocity estimation in vivo. Ultrasonics. 2010 Feb; 50(2):208–15. [PubMed: 19863987]
15. Provost J, Nguyen VT-H, Legrand D, Okrasinski SJ, Costet A, Gambhir A, et al. Electromechanical wave imaging for arrhythmias. Phys Med Biol. 2011 Nov; 56(22):1–11. [PubMed: 21119233]

16. Provost J, Thiébaut S, Luo J, Konofagou EE. Single-heartbeat electromechanical wave imaging with optimal strain estimation using temporally unequispaced acquisition sequences. Phys Med Biol. 2012 Feb 21; 57(4):1095–112. [PubMed: 22297208]
17. Provost J, Gambhir A, Vest J, Garan H, Konofagou EE. A clinical feasibility study of atrial and ventricular electromechanical wave imaging. Heart Rhythm. 2013 Jun; 10(6):856–62. [PubMed: 23454060]
18. Costet A, Provost J, Gambhir A, Bobkov Y, Danilo P Jr, Boink GJJ, et al. Electromechanical Wave Imaging of Biologically and Electrically Paced Canine Hearts in Vivo. Ultrasound Med Biol. 2014 Jan; 40(1):177–87. [PubMed: 24239363]
19. Bers DM. Cardiac excitation-contraction coupling. Nature. 2002 Jan 10; 415(6868):198–205. [PubMed: 11805843]
20. Cordeiro JM, Greene L, Heilmann C, Antzelevitch D, Antzelevitch C. Transmural heterogeneity of calcium activity and mechanical function in the canine left ventricle. Am J Physiol Heart Circ Physiol. 2004 Apr; 286(4):H1471–1479. [PubMed: 14670817]
21. Provost J, Gurev V, Trayanova N, Konofagou EE. Mapping of cardiac electrical activation with electromechanical wave imaging: An in silico–in vivo reciprocity study. Heart Rhythm. 2011 May; 8(5):752–9. [PubMed: 21185403]
22. Provost J, Lee W-N, Fujikura K, Konofagou EE. Imaging the Electromechanical Activity of the Heart in Vivo. Proc Natl Acad Sci. 2011 May 24; 108(21):8565–70. [PubMed: 21571641]
23. Costet A, Wan E, Bunting E, Grondin J, Garan H, Konofagou E. Electromechanical wave imaging (EWI) validation in all four cardiac chambers with 3D electroanatomic mapping in canines in vivo. Phys Med Biol. 2016; 61(22):8105. [PubMed: 27782003]
24. Flameng W, Schwarz F, Schaper W. Coronary collaterals in the canine heart: development and functional significance. Am Heart J. 1979 Jan 1; 97(1):70–7. [PubMed: 758746]
25. Harris AS. Delayed development of ventricular ectopic rhythms following experimental coronary occlusion. Circulation. 1950 Jun; 1(6):1318–28. [PubMed: 15414549]
26. Varghese T, Ophir J. A theoretical framework for performance characterization of elastography: the strain filter. IEEE Trans Ultrason Ferroelectr Freq Control. 1997 Jan; 44(1):164–72. [PubMed: 18244114]
27. Walker WF, Trahey GE. A fundamental limit on the performance of correlation based phase correction and flow estimation techniques. Ultrason Ferroelectr Freq Control IEEE Trans On. 1994; 41(5):644–654.
28. Luo J, Konofagou EE. High-frame rate, full-view myocardial elastography with automated contour tracking in murine left ventricles in vivo. IEEE Trans Ultrason Ferroelectr Freq Control. 2008 Jan; 55(1):240–8. [PubMed: 18334330]
29. Luo J, Konofagou E. A fast normalized cross-correlation calculation method for motion estimation. IEEE Trans Ultrason Ferroelectr Freq Control. 2010 Jun; 57(6):1347–57. [PubMed: 20529710]
30. Kallel F, Ophir J. A least-squares strain estimator for elastography. Ultrason Imaging. 1997; 19(3): 195–208. [PubMed: 9447668]
31. Bayly PV, KenKnight BH, Rogers JM, Hillsley RE, Ideker RE, Smith WM. Estimation of conduction velocity vector fields from epicardial mapping data. IEEE Trans Biomed Eng. 1998; 45(5):563–71. [PubMed: 9581054]
32. Cantwell CD, Roney CH, Ng FS, Siggers JH, Sherwin SJ, Peters NS. Techniques for automated local activation time annotation and conduction velocity estimation in cardiac mapping. Comput Biol Med. 2015 Oct 1.65:229–42. [PubMed: 25978869]
33. Scheel KW, Ingram LA, Gordey RL. Relationship of coronary flow and perfusion territory in dogs. Am J Physiol - Heart Circ Physiol. 1982 Nov 1; 243(5):H738–47.
34. Fuster, V., O'Rourke, R., Walsh, R., Poole-Wilson, P. Hurst's the Heart. 12th. McGraw-Hill Professional; 2007. p. 2200
35. Ashikaga H, Mickelsen SR, Ennis DB, Rodriguez I, Kellman P, Wen H, et al. Electromechanical analysis of infarct border zone in chronic myocardial infarction. Am J Physiol - Heart Circ Physiol. 2005 Sep 1; 289(3):H1099–105. [PubMed: 15908463]

36. Ursell PC, Gardner PI, Albala A, Fenoglio JJ Jr, Wit AL. Structural and electrophysiological changes in the epicardial border zone of canine myocardial infarcts during infarct healing. Circ Res. 1985; 56(3):436–451. [PubMed: 3971515]

37. Luke RA, Saffitz JE. Remodeling of ventricular conduction pathways in healed canine infarct border zones. J Clin Invest. 1991 May; 87(5):1594–602. [PubMed: 2022731]

38. Dillon SM, Allessie MA, Ursell PC, Wit AL. Influences of anisotropic tissue structure on reentrant circuits in the epicardial border zone of subacute canine infarcts. Circ Res. 1988 Jul 1; 63(1):182–206. [PubMed: 3383375]

39. Peters NS, Coromilas J, Severs NJ, Wit AL. Disturbed Connexin43 Gap Junction Distribution Correlates With the Location of Reentrant Circuits in the Epicardial Border Zone of Healing Canine Infarcts That Cause Ventricular Tachycardia. Circulation. 1997 Feb 18; 95(4):988–96. [PubMed: 9054762]

40. Schmidt A, Azevedo CF, Cheng A, Gupta SN, Bluemke DA, Foo TK, et al. Infarct Tissue Heterogeneity by Magnetic Resonance Imaging Identifies Enhanced Cardiac Arrhythmia Susceptibility in Patients With Left Ventricular Dysfunction. Circulation. 2007 Apr 17; 115(15): 2006–14. [PubMed: 17389270]

41. Yan AT, Shayne AJ, Brown KA, Gupta SN, Chan CW, Luu TM, et al. Characterization of the Peri-Infarct Zone by Contrast-Enhanced Cardiac Magnetic Resonance Imaging Is a Powerful Predictor of Post–Myocardial Infarction Mortality. Circulation. 2006 Jul 4; 114(1):32–9. [PubMed: 16801462]

42. Roes SD, Borleffs CJW, van der Geest RJ, Westenberg JJM, Marsan NA, Kaandorp TAM, et al. Infarct Tissue Heterogeneity Assessed With Contrast-Enhanced MRI Predicts Spontaneous Ventricular Arrhythmia in Patients With Ischemic Cardiomyopathy and Implantable Cardioverter-Defibrillator. Circ Cardiovasc Imaging. 2009 May 1; 2(3):183–90. [PubMed: 19808591]

43. Luo J, Fujikura K, Homma S, Konofagou EE. Myocardial Elastography at Both High Temporal and Spatial Resolution for the Detection of Infarcts. Ultrasound Med Biol. 2007 Aug; 33(8):1206–23. [PubMed: 17570577]

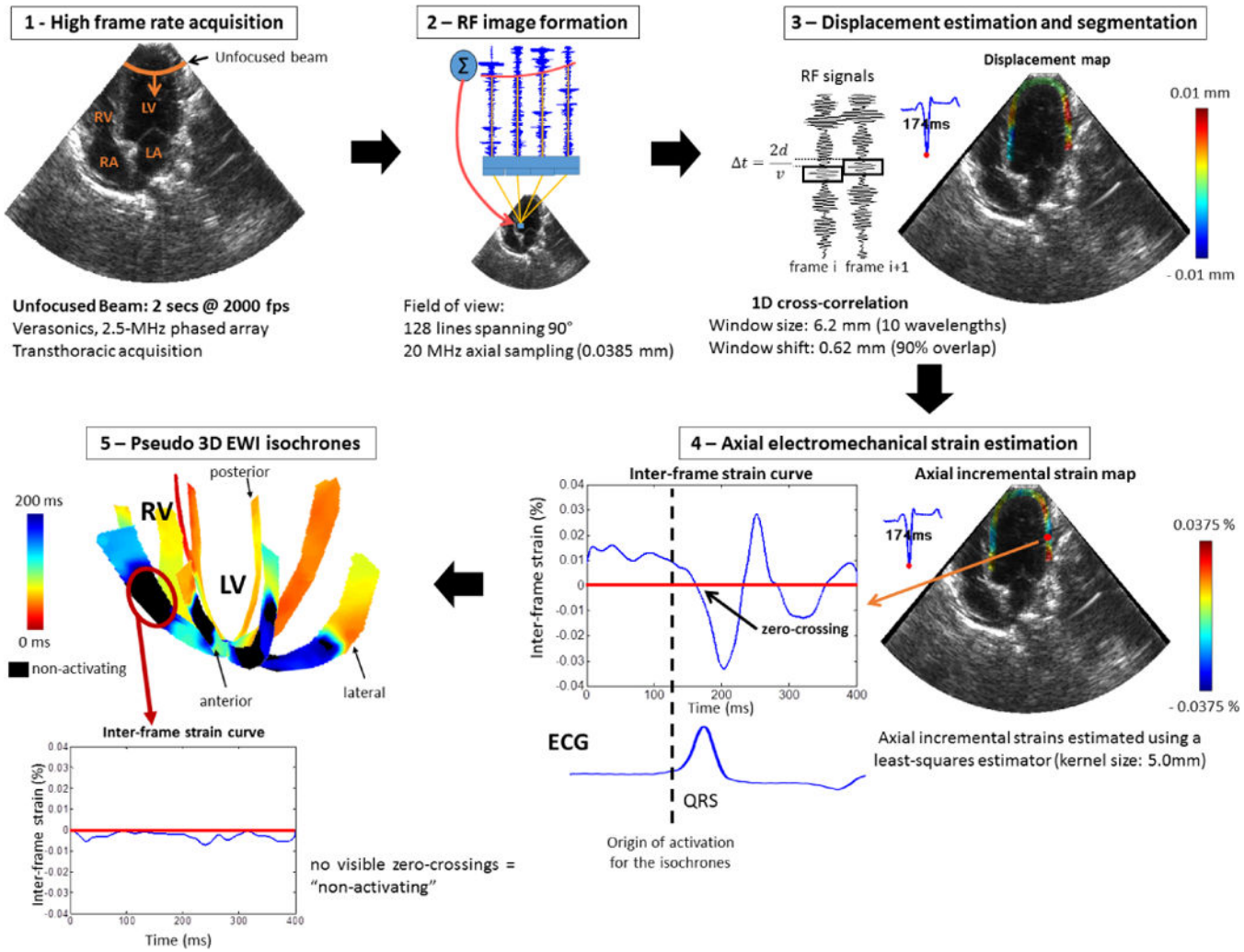

Figure 1. EWI acquisition and motion and strain estimation flowchart

(1) 2 seconds high frame-rate acquisition (2000 Hz) in standard apical views with an unfocused transmit sequence. (2) RF image formation using elements data. (3) Segmentation and 1D axial displacement estimation using 1D cross-correlation. Motion maps are generated. (4) Axial incremental strain estimated using a least-square estimator. (5) EWI isochrones are obtained semi-manually by mapping all the zero-crossings within the mask for each apical view and pseudo 3D isochrones are generated. Non-activating regions do not present a zero crossing during the cardiac cycle. LV = left ventricle, RF = radio-frequency, RV = right ventricle.

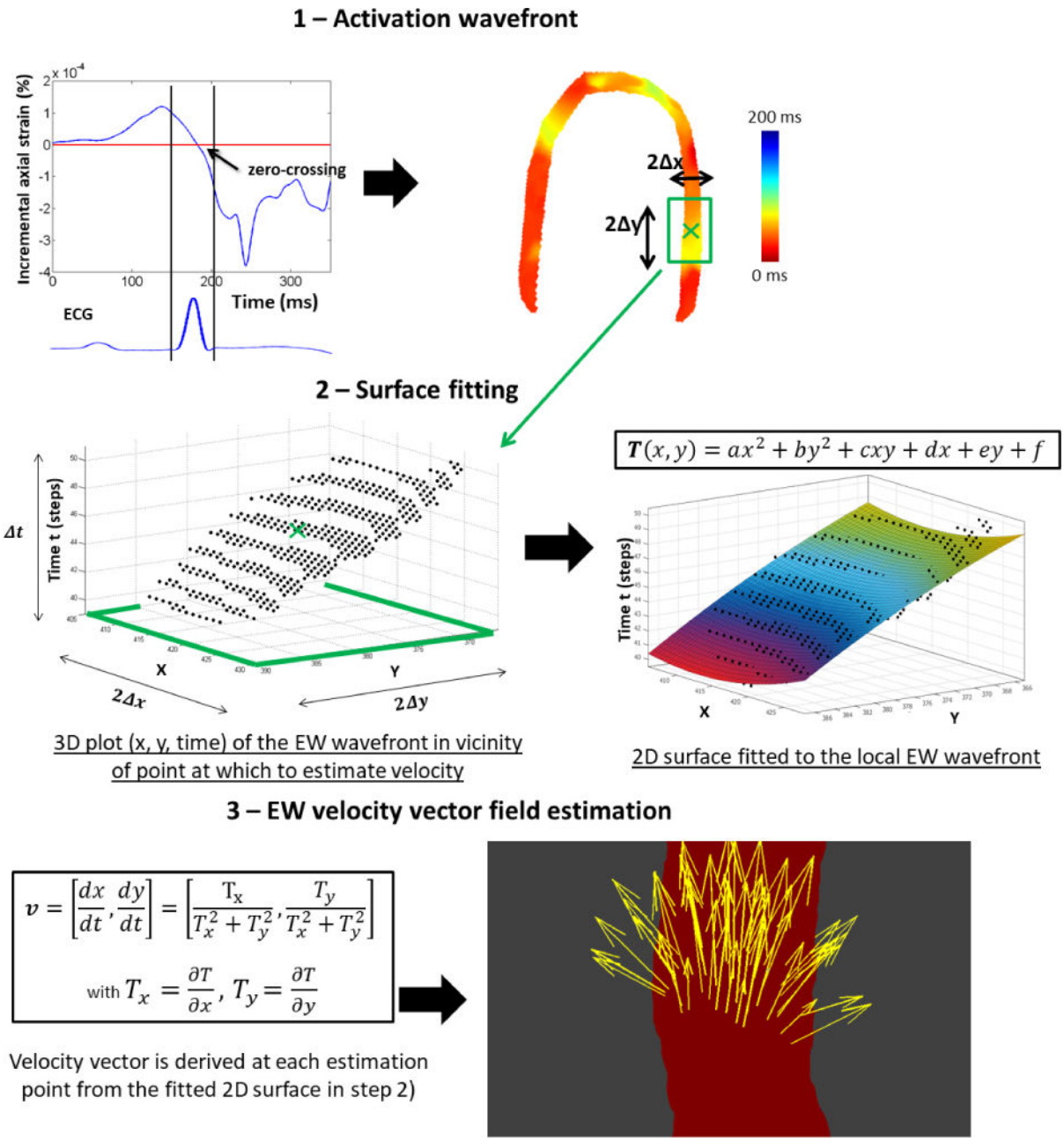

Figure 2. Block diagram of EW velocity processing

(1) The activation wavefront is determined by the zero-crossing timings within the region of interest. (2) Smooth polynomial surface fitting to active points, i.e. points on the EW wavefront. (3) EW velocity vector field estimation and video generation. EW = Electromechanical Wave.

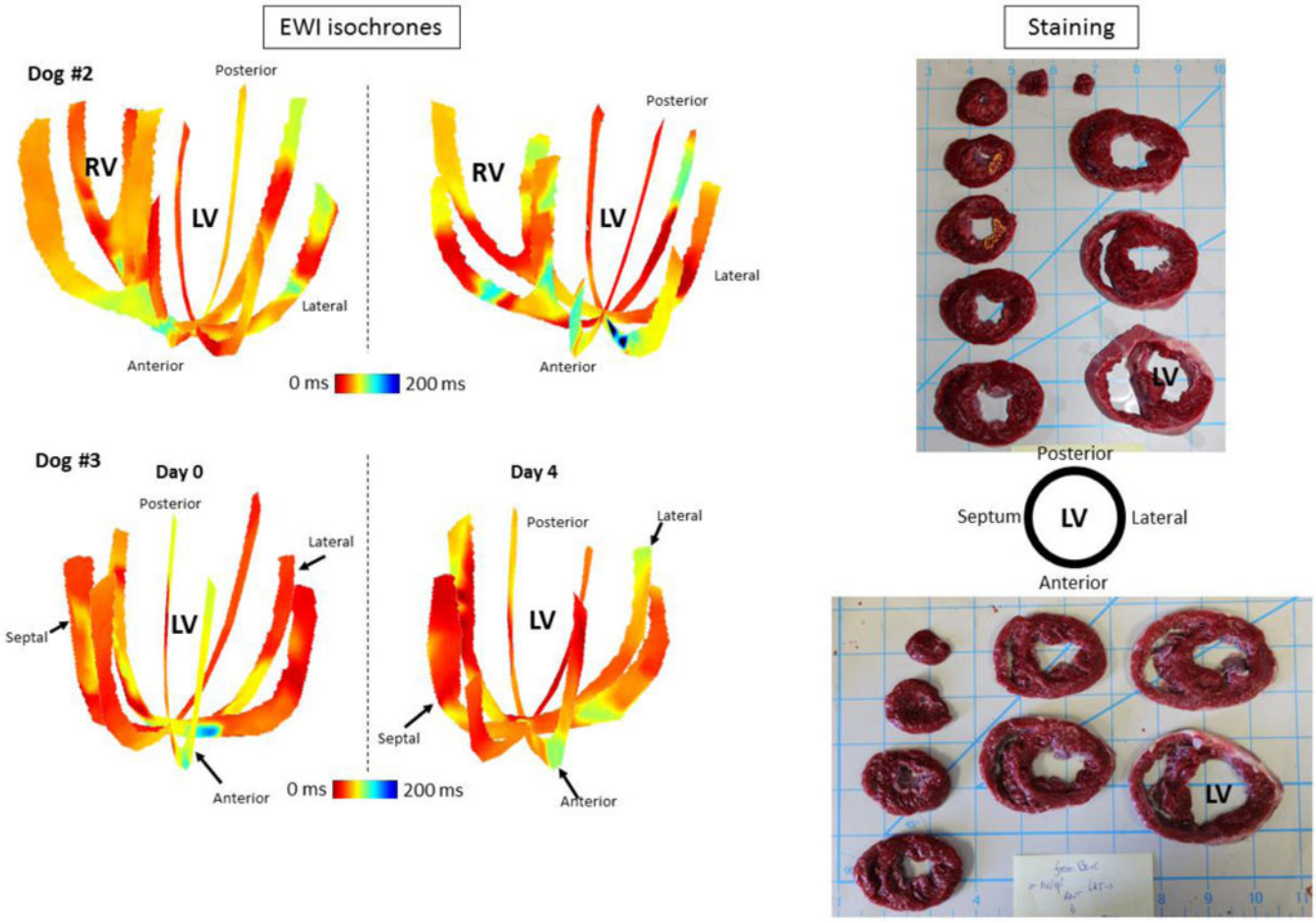

Figure 3. EWI results in dogs #2 and #3

EWI was acquired before LAD ligation and each day during the monitoring period until sacrifice on day 4 and EWI isochrones for day 0 and day 4 are shown on the left. Day 0 and day 4 isochrones for both dogs do not show marked differences in activation times. Staining results, presented on the right, reveal no significant discoloration of tissue, implying that no major infarct was formed following LAD ligation. Note that dog #2 had minor discoloration of tissue suggesting a very limited infarcted region. LAD = left anterior descending coronary artery, LV = left ventricle, RV = right ventricle.

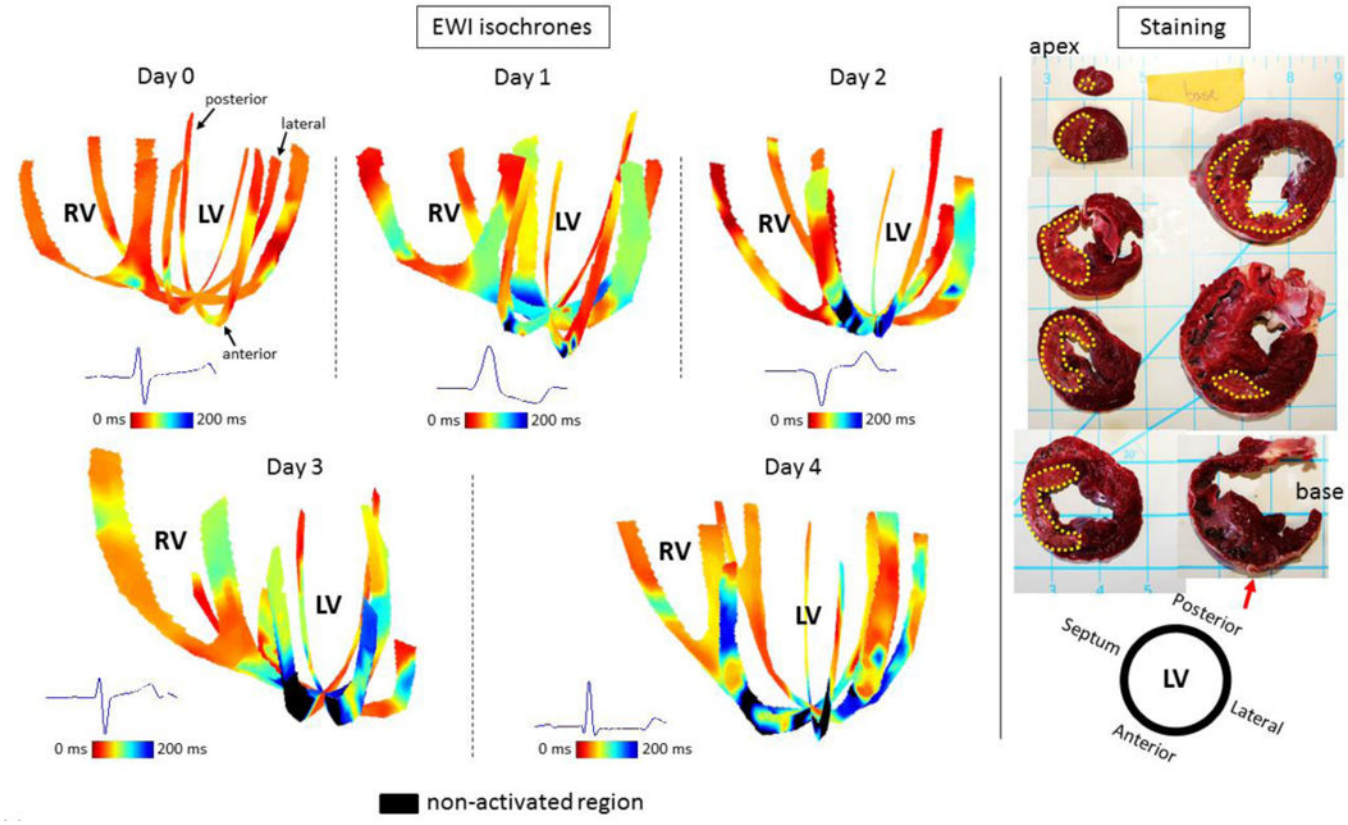

Figure 4. EWI results in dog #1

EWI was acquired before LAD ligation and each day during the monitoring period, until sacrifice on day 4. As soon as day 1, EWI isochrones on the left show late-activated (in blue) and non-activated regions (in black). Staining on the right shows regions of infarct delimited by the yellow dashed line, while a red arrow points to the location of the ligation. LAD = left anterior descending coronary artery, LV = left ventricle, RV = right ventricle.

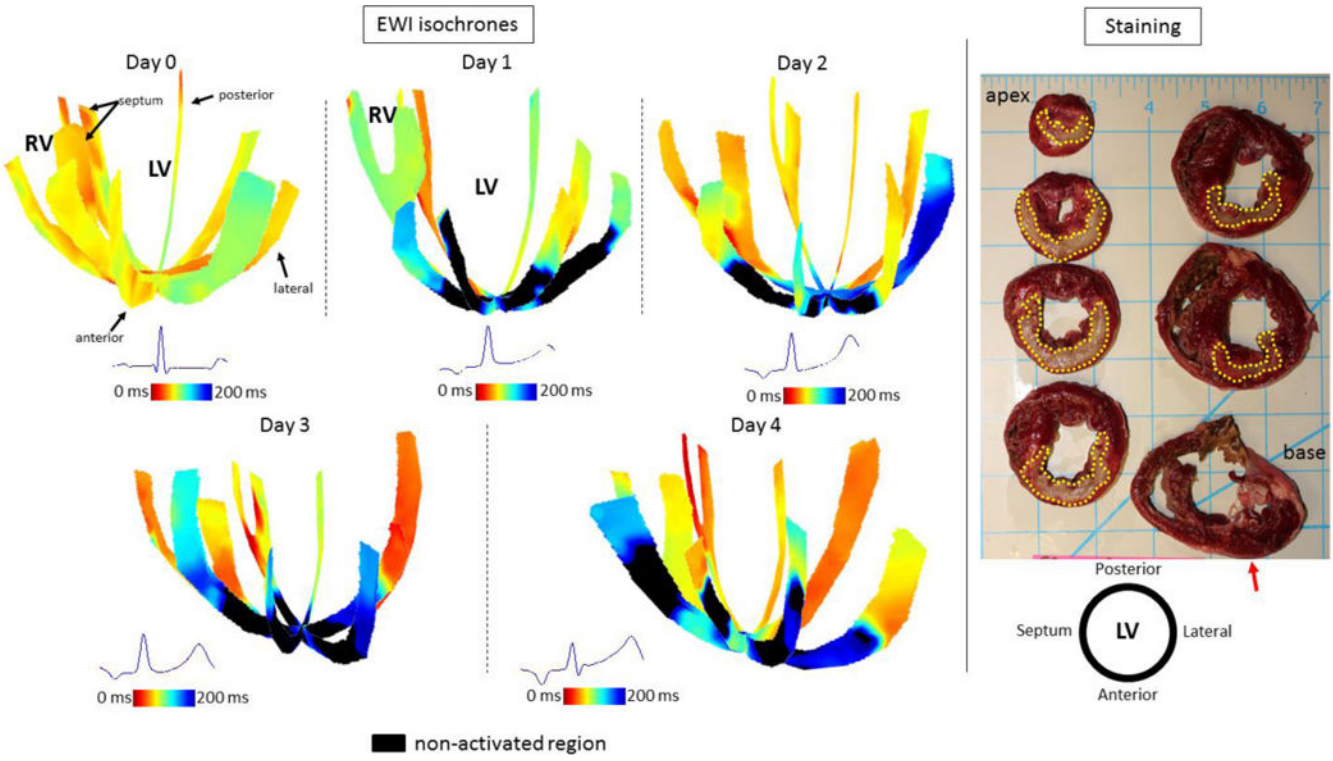

Figure 5. EWI results in dog #4

EWI was acquired before LAD ligation and each day during the monitoring period, until sacrifice on day 4. As soon as day 1, EWI isochrones on the left show late-activated (in blue) and non-activated regions (in black). Staining on the right shows regions of infarct delimited by the yellow dashed line, while a red arrow points to the location of the ligation. LAD = left anterior descending coronary artery, LV = left ventricle, RV = right ventricle.

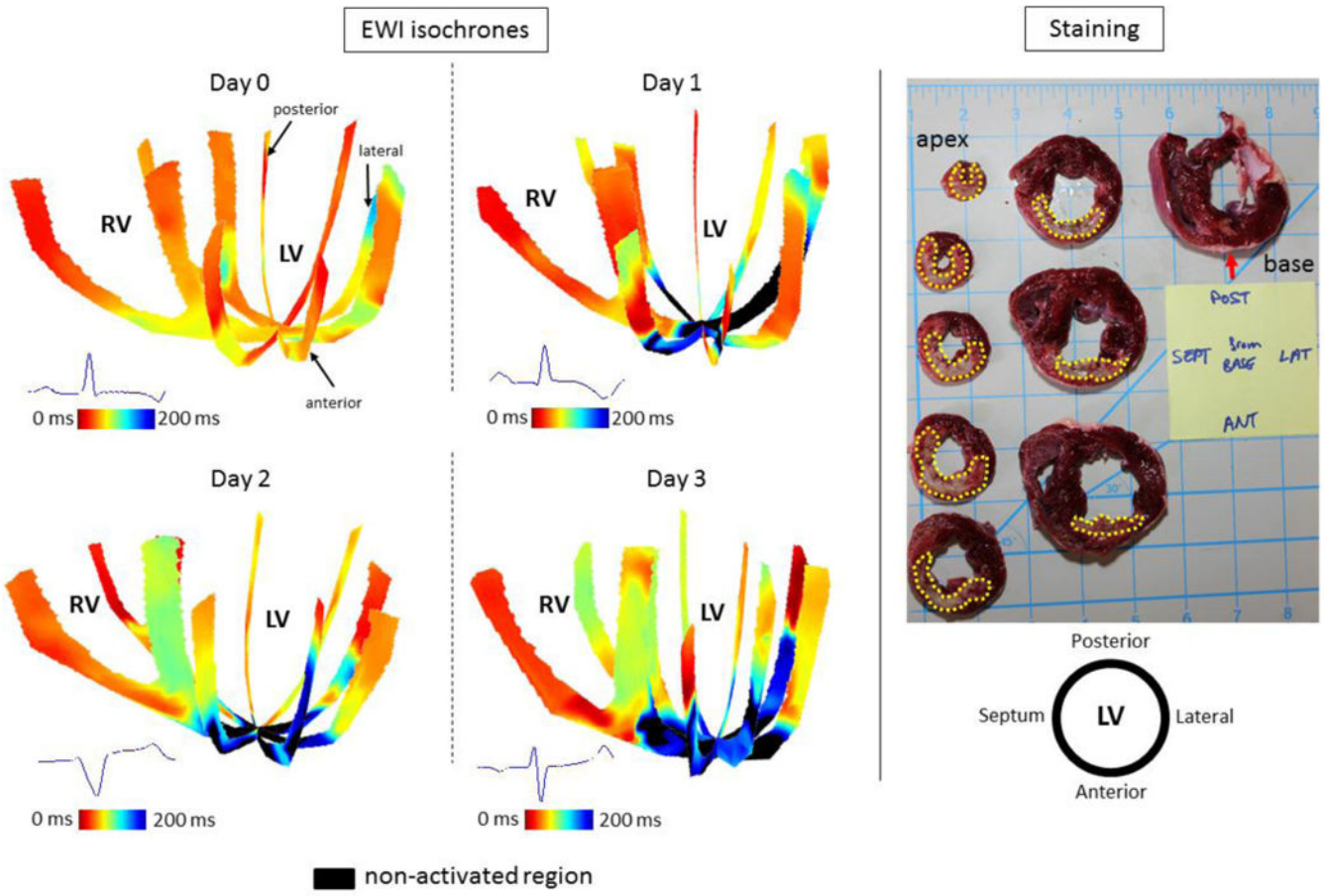

Figure 6. EWI results in dog #5

EWI was acquired before LAD ligation and each day during the monitoring period, until sacrifice on day 4. As soon as day 1, EWI isochrones on the left show late-activated (in blue) and non-activated regions (in black). Staining on the right shows regions of infarct delimited by the yellow dashed line, while a red arrow points to the location of the ligation. LAD = left anterior descending coronary artery, LV = left ventricle, RV = right ventricle.

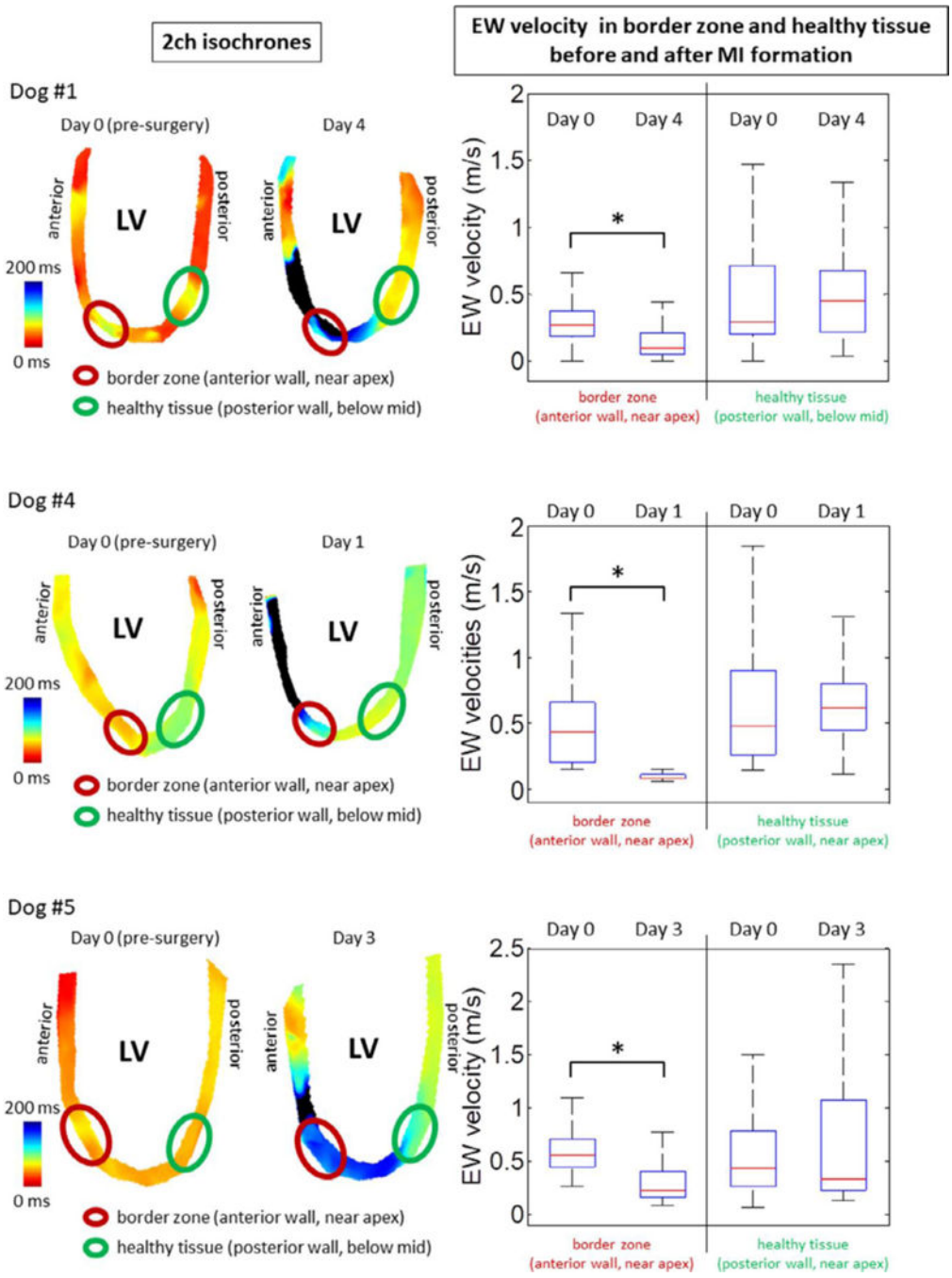

Figure 7. EW velocities in healthy region (green) and border zones of infarct (red) prior and after infarct formation

2-chamber views of the heart are presented on the left. Values of the EW velocity for regions of interest (circles on the isochrones) are compared on the right. * denotes significance ($p < 0.05$). EW = electromechanical wave, LV = left ventricle